Planetary and Space Science 71 (2012) 106–118

Contents lists available at SciVerse ScienceDirect

Planetary and Space Science

journal homepage: www.elsevier.com/locate/pss

Test-field for evaluation of laboratory craters using a Crater Shape-based interpolation crater detection algorithm and comparison with Martian and Lunar impact craters

Goran Salamunićcar [a,b,*], Sven Lončarić [b], Dejan Vinković [c], Damir Vučina [d], Mladen Gomerčić [e], Igor Pehnec [d], Marin Vojković [c], Tomislav Hercigonja [f]

[a] AVL-AST d.o.o., Av. Dubrovnik 10/II, 10020 Zagreb-Novi Zagreb, Croatia
[b] Faculty of Electrical Engineering and Computing, University of Zagreb, Unska 3, 10000 Zagreb, Croatia
[c] Physics Department, Faculty of Natural Sciences and Mathematics, University of Split, Nikole Tesle 12, HR-21000 Split, Croatia
[d] Faculty of Electrical Engineering, Mechanical Engineering and Naval Architecture, University of Split, Ruđera Boškovića 32, HR-21000 Split, Croatia
[e] GOM Gesellschaft für Optische Messtechnik mbH, Mittelweg 7-8, DE-38106 Braunschweig, Germany
[f] Topomatika d.o.o., Ilica 231, HR-10000 Zagreb, Croatia

ARTICLE INFO

Article history:
Received 29 January 2012
Received in revised form
27 June 2012
Accepted 16 July 2012
Available online 23 July 2012

Keywords:
Mars
Moon
Surface
Cratering
Laboratory crater
Crater detection algorithm

ABSTRACT

Impact craters are some of the most abundant geological features on most lunar and planetary bodies, providing insight into the history and physical processes that shaped their surface. It is therefore not surprising that extensive research has been done in the past on laboratory craters, as well as on crater detection algorithms (CDAs). No prior work has investigated how CDAs can assist in the research of laboratory craters, nor has an alternative formal method for evaluation of the similarity between laboratory and real impact craters been proposed. The result of this work is a test-field for evaluation of laboratory craters which includes: (1) a procedure for creation of explosion-induced laboratory craters in stone powder surfaces; (2) a method for 3D scanning of laboratory craters using a GOM-ATOS-I 3D scanner; (3) a new method for emplacement of laboratory craters into the topography of a planetary body; (4) a new method for objective evaluation of laboratory craters which utilizes the CDA, the Turing test, and a new measure of similarity between laboratory and real craters; and (5) a possibility of accompanying manual evaluation of laboratory craters using 2D topographical profiles. The successful verification of the proposed test-field, using Martian and Lunar global DEMs and local high-resolution DEMs, confirmed possibilities for the proposed scientific investigations of real impact craters using laboratory craters as proxies. This cost-effective approach also promises affordable accessibility for introductory physics and astronomy laboratories.

1. Introduction

State-of-the-art image-analysis/object-recognition still does not offer an answer for how to design a crater detection algorithm (CDA) that is as robust as the scientific community would desire. This is a major motivation for several research groups that are working in this still young field, trying to achieve this goal. In general, CDAs are based on a large number of methods, including circle/ellipse detection (Cooper and Cowan, 2004; Flores-Méndez and Suarez-Cervantes, 2009; Krøgli and Dypvik, 2010), edge detections (Leroy et al., 2001; Sawabe et al., 2006) and alternatives to edge detections (Maass et al., 2011), Hough transform (Michael, 2003; Bue and Stepinski, 2007), conic section fitting and graph based edge organization (Kim et al., 2005), probability volume created by template matching (Bandeira et al., 2007), boosting (Martins et al., 2009), machine-learning (Stepinski and Urbach, 2008; Urbach and Stepinski, 2009; Stepinski et al., 2009; Ding et al., 2011; Liu et al., 2011), etc. The list of publications related to CDAs is constantly increasing (Cross, 1988; Taud and Parrot, 1992; Burl and Wetzler, 2011; Wang et al., 2011; Wan et al., 2012; Troglio et al., 2012; Bandeira et al., 2012).

The scientific research on laboratory craters has lasted even longer, with the main objective to model physical processes of creation of real impact craters. A major motivation for laboratory studies of impact craters is the relatively small number of terrestrial craters (Grieve, 1987; French, 1998), and the inaccessibility of extraterrestrial impact

* Corresponding author at: AVL-AST d.o.o., Av. Dubrovnik 10/II 10020 Zagreb-Novi Zagreb Croatia. Tel.: +385 98 890725.
E-mail addresses: gsc@ieee.org (G. Salamunićcar), sven.loncaric@fer.hr (S. Lončarić), vinkovic@pmfst.hr (D. Vinković), vucina@fesb.hr (D. Vučina), m.gomercic@gom.com (M. Gomerčić), igor.pehnec@fesb.hr (I. Pehnec), marvoj@pmfst.hr (M. Vojković), t.hercigonja@topomatika.hr (T. Hercigonja).

0032-0633/$ - see front matter © 2012 Elsevier Ltd. All rights reserved.
http://dx.doi.org/10.1016/j.pss.2012.07.021

craters. Fechtig et al. (1972) described techniques for accelerating μg-, mg- and g-sized particles to meteoroid velocities (up to 50 km/s), used in order to study Lunar craters. Schmidt and Holsapple (1980) used Boeing 600-G geotechnic centrifuge in order to study, among others, the influence of gravity on cratering. Laboratory craters have additionally been used for studying: impact spallation experiments (Polanskey and Ahrens, 1990); relationships between impact and ejection velocities (Cintala et al., 1998); depth of cracking beneath impact craters (Ahrens et al., 2001); hypervelocity impact cratering in ice (Burchell et al., 2001; Grey et al., 2001); crater formation on ice silicate mixture targets (Hiraoka et al., 2007); the differences between the results of impacts on CO_2 targets with those on H_2O ice targets (Burchell et al., 2005); marine impact events (Ormö, 2005; Milner et al., 2008); cratering in layered surfaces (Senft and Stewart, 2007); effects of target properties (Barnouin-Jha et al., 2007); ejecta emplacement of Martian craters (Suzuki et al., 2007); crater excavation and formation of an uprange forbidden zone in an oblique impact (Herrick et al., 2008); ejecta fragmentation in impacts into gypsum and water ice (Miljković et al., 2011), etc. How to apply laws obtained using laboratory craters to real impact craters is certainly one of the most challenging issues. Hence, a possibility of using laboratory craters as a proxy to real ones has also been intensively studied (Desai et al., 2007, 2008; Ransom, 2011). One of the results is that even at μm scale it is possible to create simple and complex craters in laboratories (Desai et al., 2010). It is expected that different approaches to numerical modeling of impact events will contribute to these issues in future (Collins et al., 2005; Davison et al., 2011).

No previous work has investigated whether it is possible to use CDAs for the evaluation of laboratory craters. Additionally, all previous evaluations of laboratory craters have been done manually, which certainly has a disadvantage—subjectivity of the approach. This was a motivation for our investigation of the possibility of using CDAs for evaluation of laboratory craters. The preliminary results have been recently presented (Vojković et al., 2010a, 2010b; Salamunićcar et al., 2010; Vinković et al., 2011), while the completed results are given in this paper. In order to provide reproducibility of the methods presented in this paper, 3D scans of our laboratory craters and the source code (Craters5_81.-zip) of the interpolation-based CDA used in this paper have been made available online (Salamunićcar and Lončarić, 2011). In Section 2 we present methods and datasets of this paper in detail. The results of our study are presented in Section 3 and the conclusion is given in Section 4.

2. Methods and datasets

2.1. Creation of explosion-induced laboratory craters in stone powder surfaces

The experiments were performed on fine dry stone powder surfaces of a material with negligible strength, produced in a local limestone quarry as a by-product of stone cutting. The usage of stone powder instead of hard rock targets gives a possibility to simulate large-scale events with small amounts of explosive charges, as explained in Section 3.1. The powder was placed in containers much larger than the finally obtained craters. The powder was compressed so that the surface density was 1.5–1.9 g/cm^3, as shown in Table 1. In our case, the silver acetylide (Ag_2C_2) explosive charge was used for crater formation. Cylindrically shaped charges were buried just below the surface. The charge mass was 105–350 mg and the cylinder height/width was 0.375–1.5, as shown in Table 1. Explosive charges were ignited using a laser. We used silver acetylide for explosive charges because it is easily accessible in small quantities as a by-product of regular chemistry classes. One of our objectives was similar to the work by Kasas et al. (2000) and Claycomb (2009)—the creation and study of craters to be affordable to low-budget laboratories, and with this to a large number of students.

2.2. Scanning of laboratory craters using a 3D scanner

Laboratory craters were scanned in 3D to produce a high-accuracy digital topography of their shape. The device GOM-ATOS-I used for digitizing the craters is based on the principle of stereo-photogrammetry, which projects structured light patterns onto the surface of the object and captures the image using two CCD cameras, each with a resolution of 1032×776 pixels. Different line patterns are projected onto the surface in a time sequence to enable simple identification of the spatial positions of measurement points. Based on the stereo scans of the deformed projected lines and using triangulation, the 3D-shape of the surface is determined accordingly. More detailed description of the GOM-ATOS-I device is available online (GOM, 2012).

2.3. Turing test and measure of similarity between laboratory and real craters

The objective is to provide a formal method for measuring the similarity between laboratory and real craters. We developed an approach based on CDAs and 3D-shapes of laboratory craters which utilizes the Turing test (Saygin et al., 2000): if a laboratory crater is sufficiently similar to the real one to be detected via the CDA then we consider this to be a satisfactory model, otherwise it is rejected as insufficiently similar. In order to perform a more advanced measurement of similarity, an A-ROC (also referenced in the literature as a ROC' curve) evaluation of CDAs can be used. Each position of a laboratory crater on the A-ROC curve corresponds to a probability threshold, which defines the working mode of CDA wherein only those detections with higher assigned probability than the threshold are accepted. During detection of a laboratory crater, the CDA assigns to it a probability that it is an impact crater in the same way as for detections of real craters.

Table 1
Basic information on our laboratory craters (*explosive charge cylinder diameter is 8 mm).

Craters	Attributes				
	Surface density of used material [g/cm^3]	Explosive charge cylinder depth* [mm]	Explosive charge cylinder mass [mg]	Depth of resulting crater [mm]	Diameter of resulting crater [mm]
lab-crater-1	1.90	8	197 ± 10	15.8	49.5
lab-crater-2	1.80	11	295 ± 10	12.9	45.2
lab-crater-3	1.70	8	190 ± 10	13.1	43.8
lab-crater-4	1.80	3	105 ± 10	5.9	29.7
lab-crater-5	1.57	5	165 ± 10	9.5	39.2
lab-crater-6	1.75	5	179 ± 10	10.7	41.8
lab-crater-7	1.75	12	350 ± 10	21.7	61.3

This defines its position on the A-ROC curve, where the probability assigned to a laboratory crater is equal to the probability threshold. When a crater is closer to the bottom-left corner of the A-ROC curve, it is detected with larger associated probability that it is indeed a crater, and therefore its 3D-shape is more similar to real craters. In our case, as a measure we use a percentage of the distance from the top-right corner to the position of a laboratory crater on the A-ROC curve, as defined with Eq. (1) (for definitions of TDR and FDR see Table 2). If, on the contrary, a similarity between laboratory crater and some particular real crater is required, a percentage of the distance between the position of a laboratory crater on the A-ROC curve and the position of a real crater on the A-ROC curve can be used:

$$p_{lc} = \sqrt{\frac{(1-TDR)^2+(1-FDR)^2}{2}} \quad (1)$$

Table 2
Definitions and graphs (TP = true positives; FP = false positives; FN = false negatives; GT = ground truth; TDR = true detection rate; FDR = false detection rate; ROC = receiver operating characteristics; F-ROC = free-response ROC; A-ROC = approximation of ROC) used for evaluation of CDAs (Salamunićcar et al., 2012).

Used definitions	**Used graphs [horizontal range/vertical range]**
GT = TP + FN TDR = TP/(TP + FN) = TP/GT FDR = FP/(TP + FP)	F-ROC [TP/FP] A-ROC [TDR/FDR]

2.4. *Emplacement of laboratory craters in the topography of a planetary body*

In order to perform the Turing test, including measurement of similarities between laboratory and real craters, 3D-scans of laboratory craters need to be emplaced in the topography of a planetary body. The objective for emplacement is to provide a smooth transition between the surrounding topography and a laboratory crater, and at the same time to preserve the topography of the laboratory crater. The four major steps of the method are as follows:

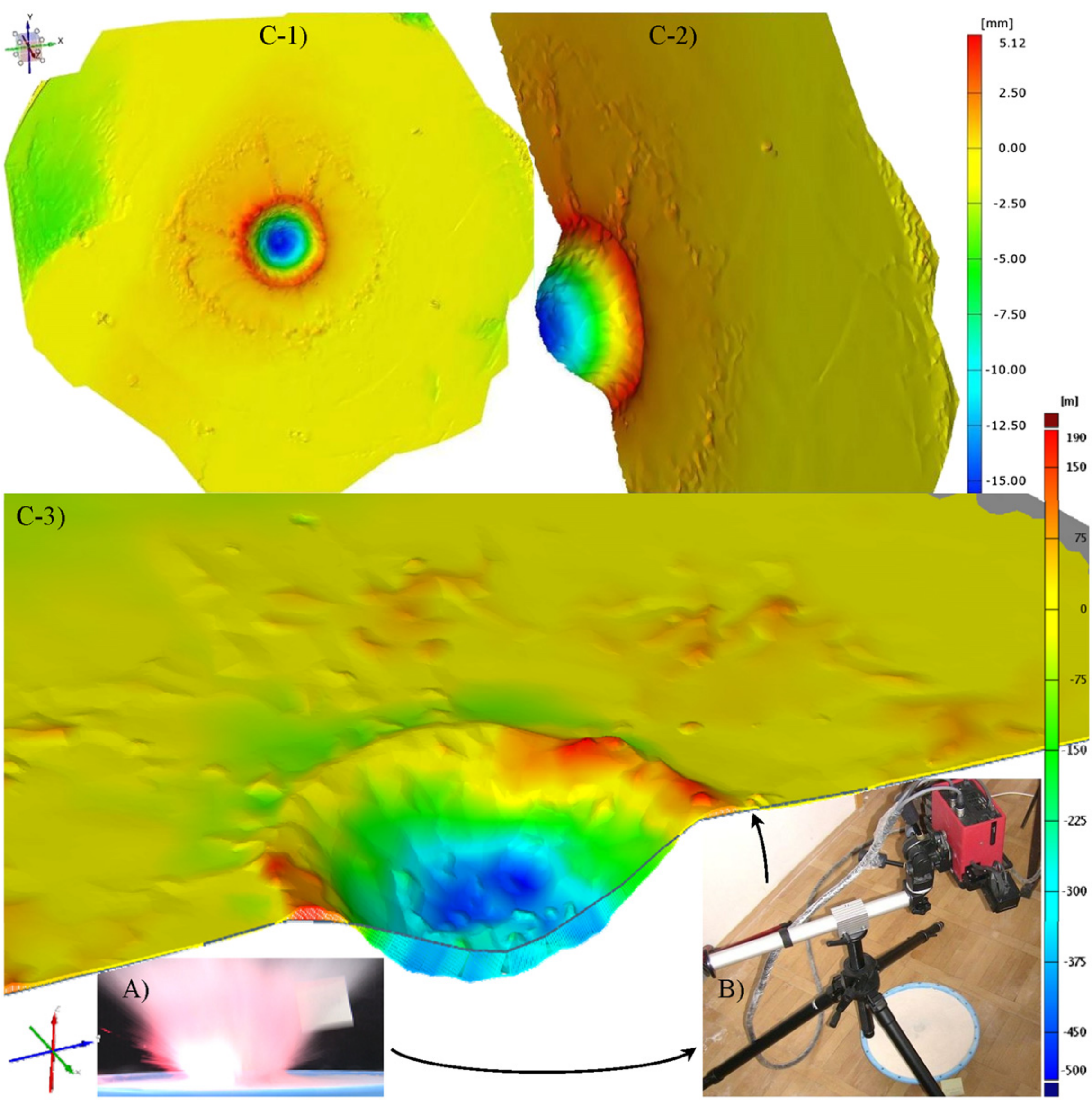

Fig. 1. Scanning of an explosion-induced laboratory crater (A) using a 3D scanner (B), resulting profiles (C-1 and C-2), and comparison of our laboratory crater and Martian crater S027098B13104K01753T56623Y2007S (D = 5.1 km) from MA132843GT catalog rendered using 1/128° MOLA data (C-3).

(1) identification of rectangles associated with the coordinates (top, bottom, left, and right) of each individual laboratory crater (in the following text: object-rectangle); (2) compensation for values close to the rectangle's edges with smoothing (in the following text: correction-1); (3) smoothing of places where laboratory craters will be emplaced (in the following text: correction-2); and (4) creation of a transition mask between the laboratory crater and the background topography (in the following text: transition-mask). The summary of the method is as follows: (1) it takes values from a laboratory crater's 3D-scan; (2) they are decreased with correction-1 values; (3) they are increased with correction-2 values; (4) the transition-mask's values are used for interpolation between the values computed in the previous step and the values of background topography. The objective of correction-1 is to prevent sharp transition between the background topography and an emplaced laboratory crater. The objective of correction-2 is to prevent superposition of the geological features from the background topography to the shape of the laboratory crater. The objective of the transition-mask is to provide a smooth transition between surrounding topography and the laboratory crater.

Each object-rectangle is defined as the smallest rectangle, with the first and last row and column containing at least one value different from 0. The algorithm for correction-1 and correction-2 is as follows. In the first step, correction values are defined, such that the distance to object-rectangle is 1, 2 or 3 pixels, as an average value for masks sized 3×3, 5×5 and 7×7 pixels, respectively. In the second step the remaining correction values are defined, using values at the distance of 3 pixels from the object-rectangle. They are averaged using a weight factor that is inversely proportional to d^4, where d is the distance in pixels from the pixel of interest to the used correction value. The algorithm for the transition-mask is as follows. Within each object-rectangle two rectangles are defined with rounded corners. For values outside the larger of these, background topography values will

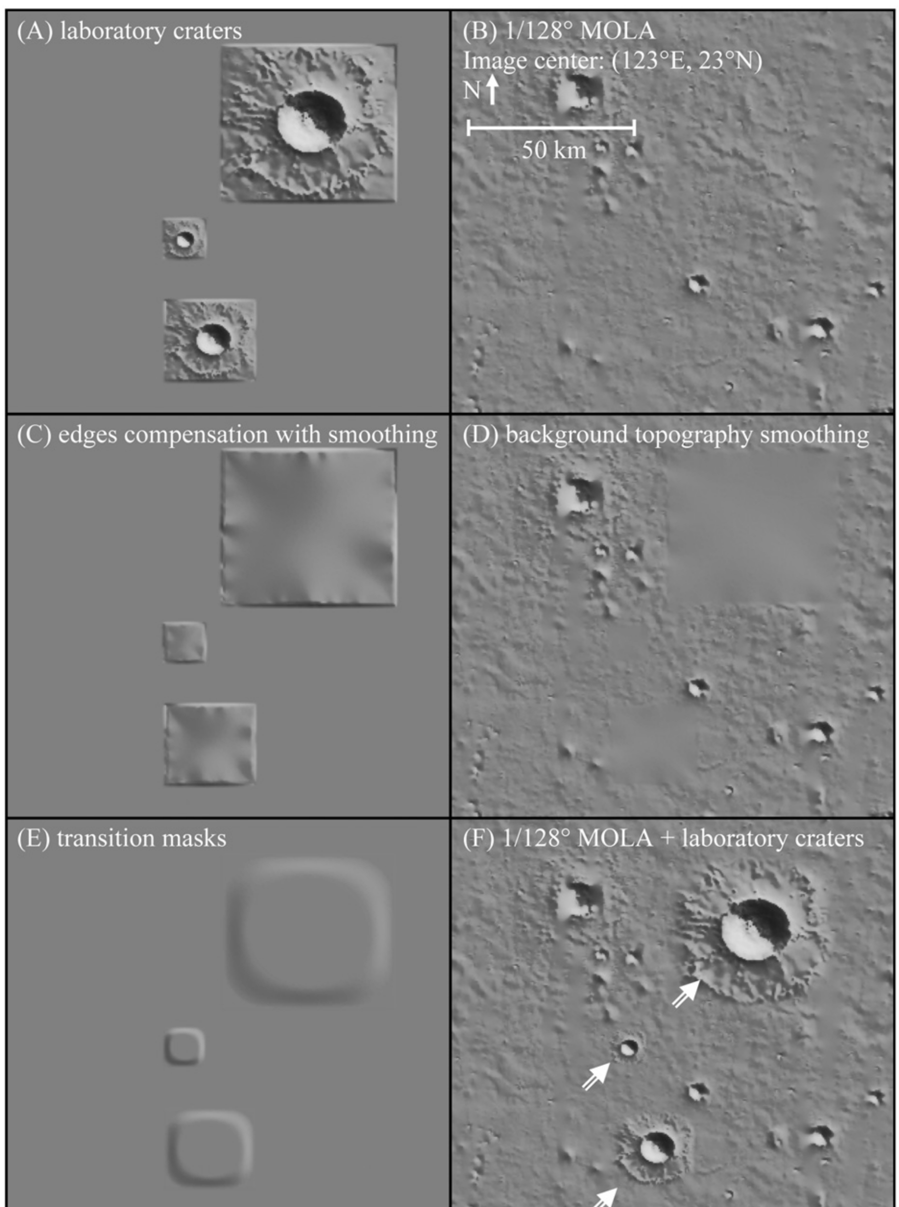

Fig. 2. Steps of laboratory crater emplacement: (A) 3D-scans of laboratory craters; (B) background topography; (C) compensation of values close to edges with smoothing; (D) smoothing of places where laboratory craters will be emplaced; (E) transition masks between laboratory craters and background topography; and (F) emplaced laboratory craters.

be used as final without modification. For values inside the smaller, processed values of the laboratory crater's 3D-scan will be used as final without modification. For values between the two rectangles with rounded corners, linear interpolation is used to provide transition between two digital elevation maps (DEMs).

2.5. *Crater detection algorithms and extraction of topographical profiles of laboratory craters*

In our previous work, we developed a CDA for crater detection from digital topography data using gradient value/orientation, morphometry, votes-analysis, slip-tuning and calibration (Salamunićcar and Lončarić, 2010; in the following text: CDA_1) and further improved it using a Crater Shape-based interpolation (Salamunićcar et al., 2012; in the following text: CDA_2). Both versions use: (1) multi-resolution image analysis; (2) various edge-detection methods, with the best results provided by Canny (in the following text: CDA_1-Canny and CDA_2-Canny) and by Shen-Castan (in the following text: CDA_1-Shen-Castan and CDA_2-Shen-Castan); and (3) the Hough transform (also referenced in the literature as a Radom-Hough transform). Once the 3D-shape of a laboratory crater is emplaced in e.g. Martian or Lunar topography, the CDA can also be used to extract profiles of laboratory craters in the same way as for real craters. Such an approach ensures that profiles of real and laboratory craters are extracted in the same way, and with this prepared for further analysis.

2.6. *Datasets used for test-fields*

We used datasets prepared in our previous work (Salamunićcar et al., 2012) based on Mars orbiter laser altimeter (MOLA) dataset (Smith et al., 2003) and Lunar orbiter laser altimeter (LOLA) dataset (Smith et al., 2010). Additionally, we used some high-resolution Martian and Lunar DEMs.

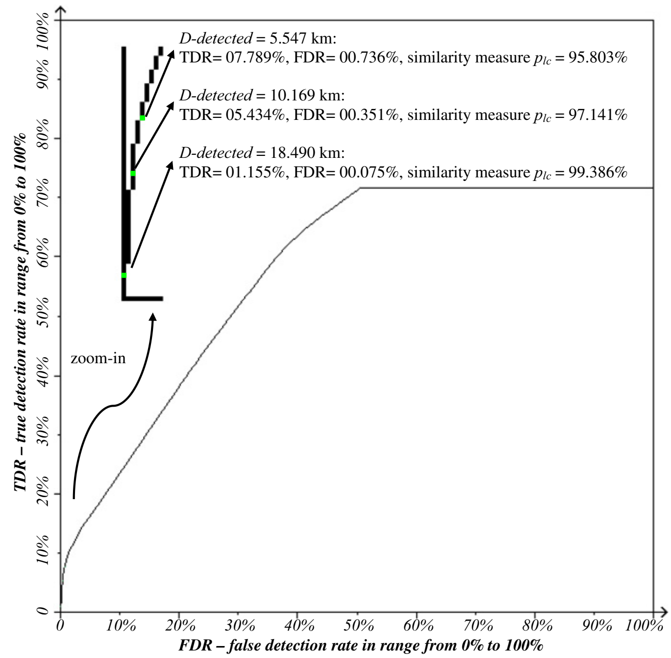

Fig. 4. An example of the estimation of the similarity between laboratory and real impact craters using Eq. (1) and the A-ROC evaluation of CDAs based on true and false detection rates.

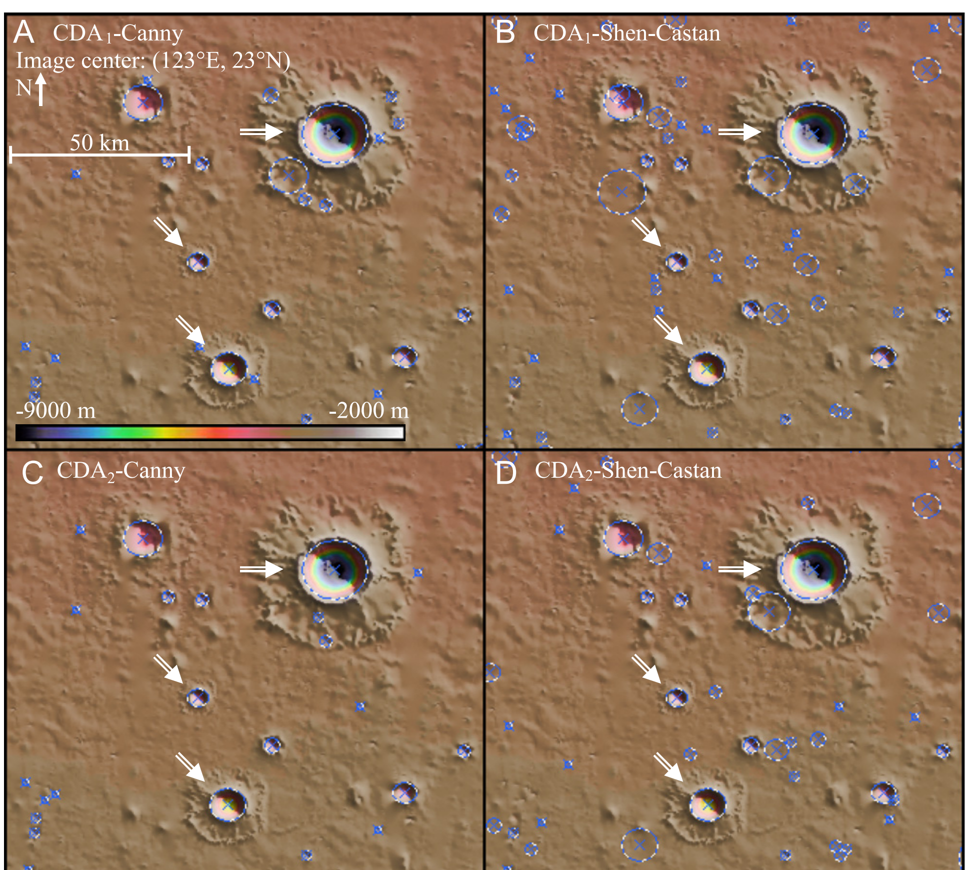

Fig. 3. Detections of laboratory craters in the context of the real topography using: (A) CDA_1-Canny; (B) CDA_1-Shen-Castan; (C) CDA_2-Canny; and (D) CDA_2-Shen-Castan.

3. Results and discussion

3.1. Basic properties of laboratory craters created

Craters on planetary and lunar surfaces display a simple–complex transition from the smaller, mostly very circular bowl-shaped craters, to larger complex craters with central peaks, and to the largest multi-ring impact basins (Melosh and Ivanov, 1999). The theory of simple impact craters distinguishes between the strength regime and the gravity regime of cratering (Holsapple, 1993, 1994). The strength regime is applied when the strength of a soil surface is large compared to the gravitational pressures within the ground surface at depths comparable to the impactor size. Under such conditions the crater shape is dictated by the soil properties. The gravity regime is applicable when the soil strength is much smaller than the gravity pressure. Under that regime the crater shape is dictated by the impactor's size and velocity for a given planet surface gravity. It is exactly the gravity regime that we encounter in the case of asteroidal impactors, where kinetic energy is large enough to ignore the soil strength. At the instant of impact, large volumes of target rock are shattered, deformed, melted, and even vaporized in a few seconds (French, 1998). An object only a few meters across ($\sim$6 m) carries the kinetic energy of an atomic bomb (Hiroshima, Japan $\sim$20 kT of TNT equivalent) and results in a considerably larger crater ($D=120$ m) while the energy release in an impact event is virtually instantaneous (French, 1998). The immediate energy release can be treated with the classical physics of point source explosions where the actual source of energy is irrelevant. This approach has been used to successfully explain the morphology of impact craters (Holsapple, 1993). Alternatively, we can enable the gravity regime if the soil strength is close to zero, such as in our stone powder material, while the point source explosion is induced by an explosive charge of lower yield than actual asteroid impacts. The results show that our experimental cratering can be used as a proxy for simple Martian and Lunar craters formed under the gravity regime, even though depths of our laboratory craters are 5.9–21.7 mm and diameters are 29.7–61.3 mm, as shown in Table 1.

3.2. Resulting 3D-scans of laboratory craters created

An example of a 3D-scan of an explosion-induced laboratory crater is shown in Fig. 1. A comparison with a similar profile of a Martian crater with a high depth/diameter ratio is also shown. As can be seen, the 3D-scans are highly accurate representations of craters' shapes. In addition, the scans show that our laboratory craters contain a well formed crater rim, as well as crater ejecta blanket at a distance between rim and approximately two craters' radii. Accordingly, at least the most important morphological properties of simple craters can be modeled in a laboratory and accurately digitalized for further analysis and comparison with real impact craters.

3.3. Results of laboratory craters' emplacement for three different sizes

The method for emplacement of a laboratory crater's 3D-scan works satisfactorily, as shown in Fig. 2. The transition between surrounding topography and laboratory craters is smooth, while at the same time the topography of the laboratory crater is preserved. For the purpose of method illustration, some intermediate steps are shown as well: correction-1's values in frame (C); correction-2's values in frame (D); and the transition-mask's values in frame (E). The method works successfully for different sizes, as shown in frame (F).

3.4. Results for different crater detection algorithms and accompanying evaluation

CDA_2 provides better results than CDA_1. In addition, results are better for Canny based CDAs than for those based on Shen-Castan. However, in this work we are using all four versions (CDA_1–Canny, CDA_1-Shen-Castan, CDA_2-Canny and CDA_2-Shen-Castan), because this is the best possible test of the overall robustness of the approach that can be currently performed. As shown in Fig. 3, detections via different CDAs are similar but still different.

An example of the estimation of similarity between laboratory and real impact craters using Eq. (1) and the A-ROC evaluation of CDAs is shown in Fig. 4. The same laboratory crater is scaled to three different sizes in order to test how this influences overall results. The largest one is detected via the CDA with the largest associated probability because, for larger craters, the associated large depth/diameter ratio is a stronger indication that the detected object is a crater. However, differences between these three cases are not great, as expected, because the same laboratory crater is emplaced in three different sizes.

3.5. Martian and Lunar based test-fields and resulting profiles of laboratory craters

Mathematical modeling of impact craters using parabola segments is shown in Fig. 5. With such an approach, it is possible to model simple impact craters with rim, central peak, or both. Martian and Lunar test-fields for laboratory craters are shown in

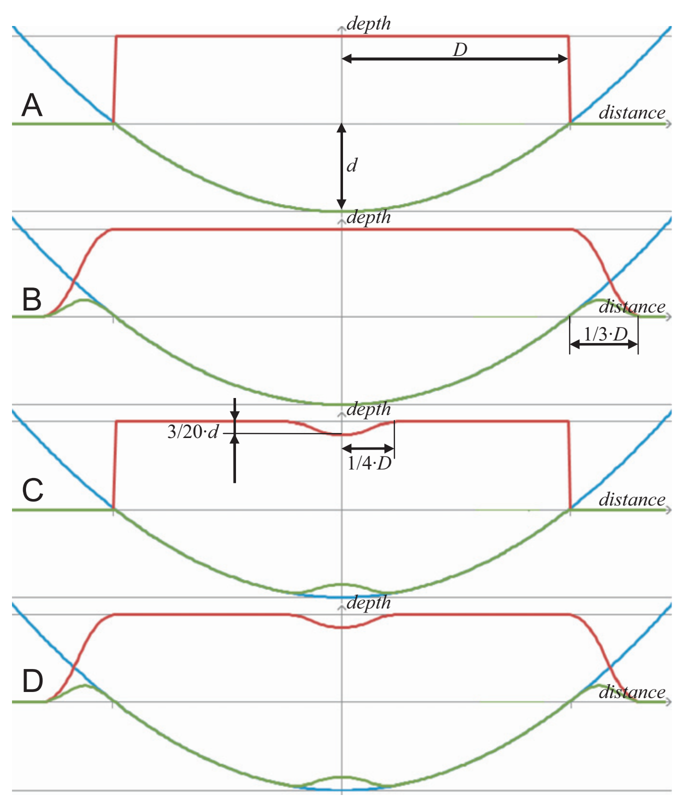

Fig. 5. Mathematical modeling of impact craters using parabola segments (functions of form $y=ax^2+bx+c$, where x is distance and y is depth), the model of an impact crater (green) is the product of basic parabola (blue) and modification function (red) which goes vertically between 0 and 1: (A) an impact crater without rim and without central peak; (B) an impact crater with rim but without central peak; (C) an impact crater with central peak but without rim; and (D) an impact crater with rim and with central peak. (For interpretation of the references to color in this figure legend, the reader is referred to the web version of this article.)

Fig. 6. In addition to laboratory craters and mathematical models, cross, triangle, quadrangle and hexagon artificial objects are used in order to test the overall approach. The basic idea is as follows: for shapes more similar to real craters, the measure of similarity should provide larger values. In principle, the results including profiles for Martian topography are similar to the results for Lunar topography, as expected. There are some smaller differences, but this is also expected for different parts of the topography of the same lunar or planetary body. In our case, we selected parts of the global topography, which is mostly flat, in order that shapes could be embedded in it without considerable distortions. Selected parts also contain some roughness, in order to evaluate how this influences the results.

3.6. Cross-comparison of detection results

Detections of CDA_2-Canny for the Martian test-field are shown in Fig.7 and for the Lunar test-field in Fig. 8. The artificial object cross is not detected in either size or test-field. The artificial objects triangle and quadrangle are detected in only some cases. The artificial object hexagon is detected in all sizes and both test-fields. According to the Turing test, the cross is insufficiently

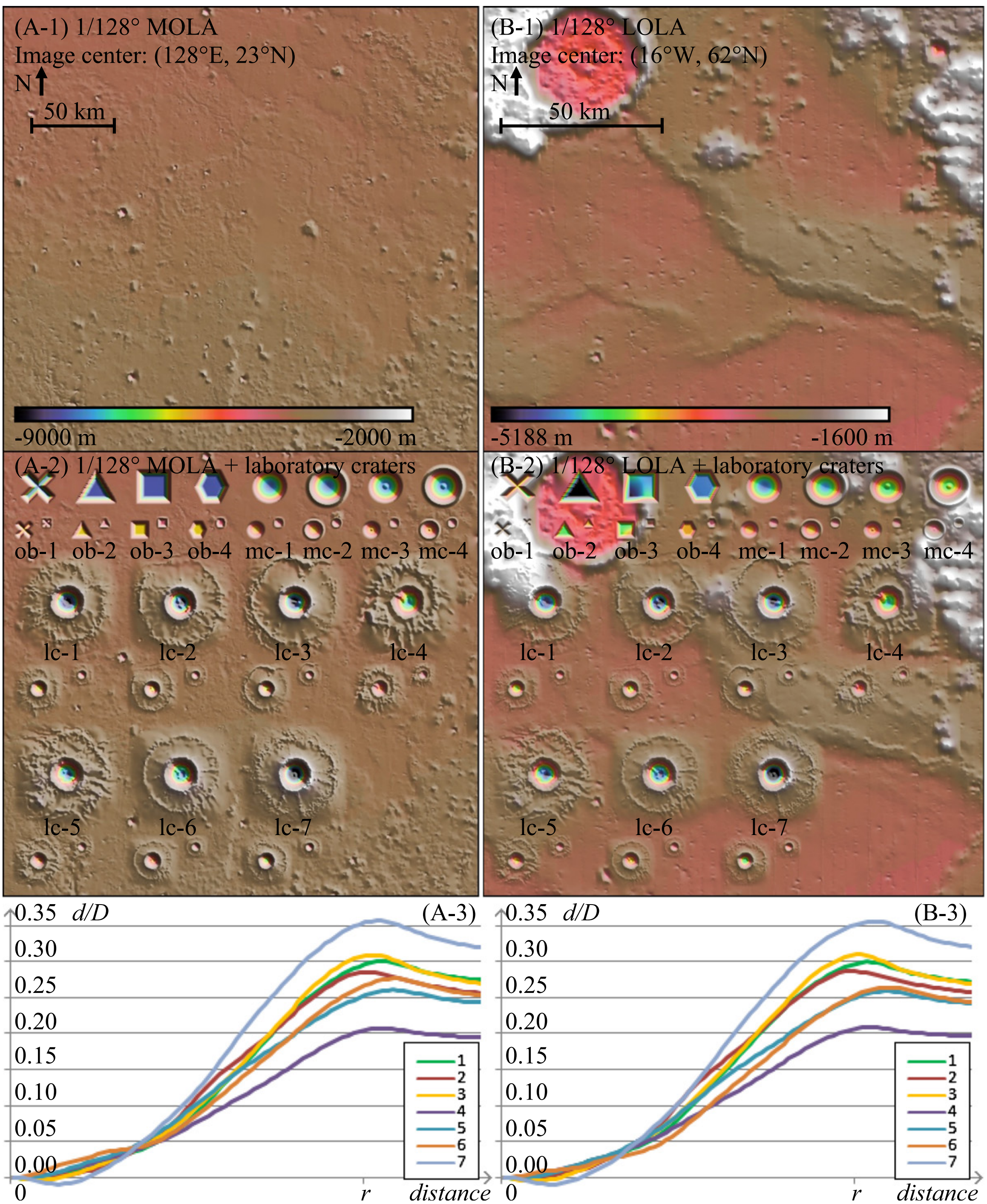

Fig. 6. Martian (A-*) and Lunar (B-*) test-field for cross, triangle, quadrangle and hexagon artificial objects (ob-*), mathematical models of craters (mc-*), and laboratory craters (lc-*): initial topography (top row), embedded diverse shapes (middle row), and profiles of laboratory craters (bottom row).

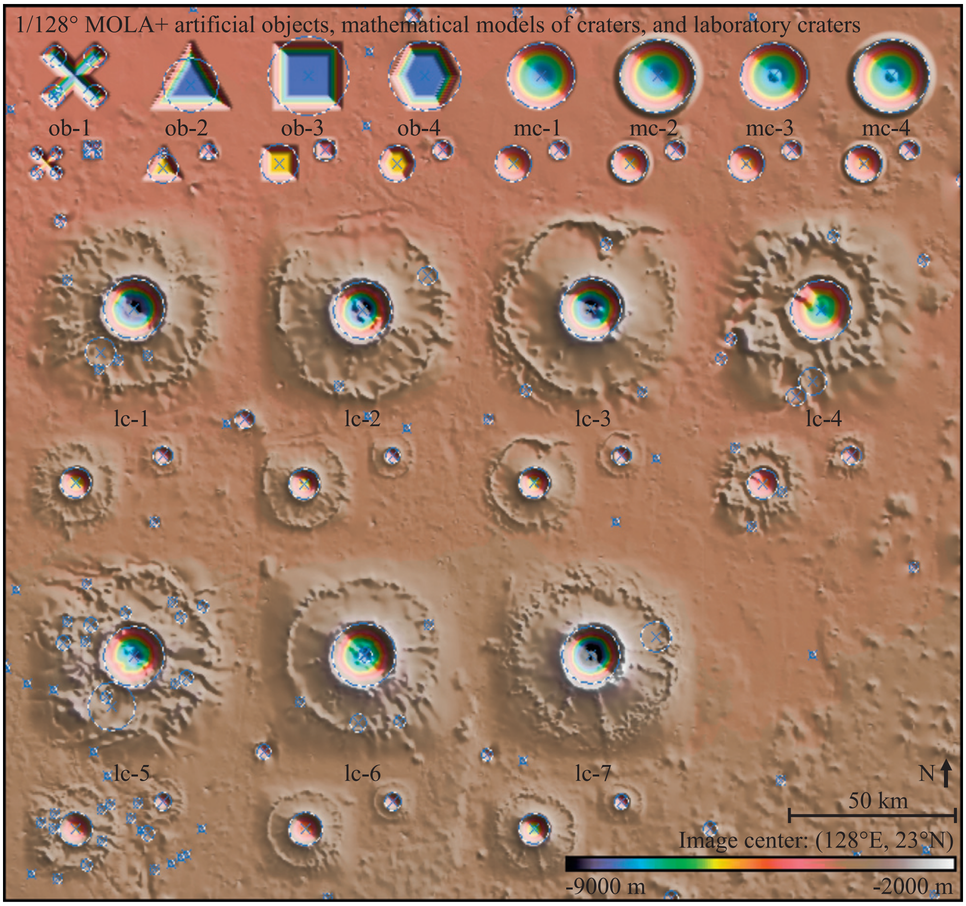

Fig. 7. Detections of cross, triangle, quadrangle and hexagon artificial objects (ob-*), mathematical models of craters (mc-*), and laboratory craters (lc-*), embedded in Martian topography, using CDA_2-Canny.

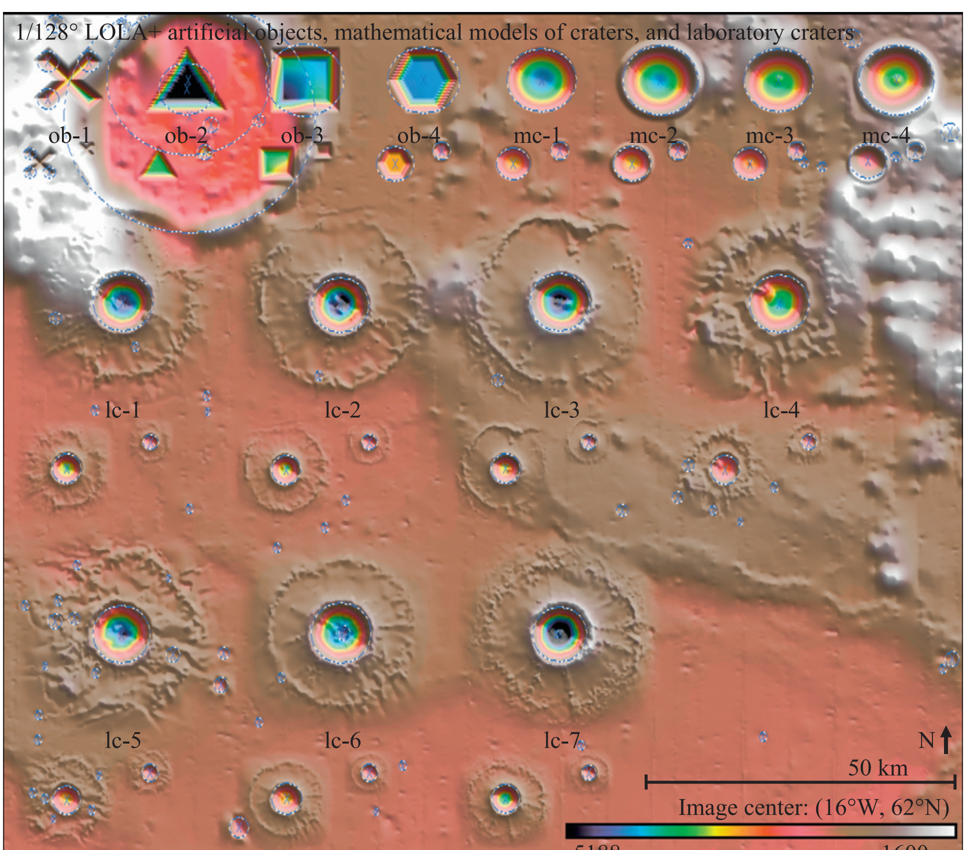

Fig. 8. Detections of cross, triangle, quadrangle and hexagon artificial objects (ob-*), mathematical models of craters (mc-*), and laboratory craters (lc-*), embedded in Lunar topography, using CDA_2-Canny.

Table 3
Results of the evaluation of artificial objects (cross, triangle, quadrangle, hexagon), mathematical models of craters (math-crater-*), and laboratory craters (lab-crater-*), for the largest size, using diverse CDA-s and topographies (X means that the Turing test failed).

Target	Test							
	Mars CDA_1-Canny (%)	Mars CDA_2-Canny (%)	Mars CDA_1- Shen-Castan (%)	Mars CDA_2- Shen-Castan (%)	Moon CDA_1-Canny (%)	Moon CDA_2-Canny	Moon CDA_1-Shen-Castan	Moon CDA_2-Shen-Castan
cross	X	X	X	X	X	X	X	X
triangle	80.812	73.686	79.756	77.512	26.686	24.092	X	X
quadrangle	91.959	90.327	94.005	93.029	31.200	31.682	49.393	44.142
hexagon	96.879	96.897	95.613	95.310	96.733	96.349	85.760	85.694
math-crater-1	99.330	99.786	99.880	99.948	98.392	98.346	90.363	92.377
math-crater-2	100.000	100.000	100.000	100.000	99.869	99.890	98.625	98.552
math-crater-3	99.355	99.643	95.142	95.074	97.632	97.026	72.393	74.967
math-crater-4	100.000	100.000	100.000	100.000	99.872	99.873	99.259	99.329
lab-crater-1	98.924	99.634	98.962	99.065	96.403	96.482	87.092	89.862
lab-crater-2	99.657	99.933	98.808	99.517	99.374	99.559	98.105	98.432
lab-crater-3	99.440	99.725	98.957	99.269	99.225	99.286	97.281	96.909
lab-crater-4	97.854	98.492	99.212	99.455	97.752	97.786	95.006	96.549
lab-crater-5	98.817	99.126	97.502	97.888	98.780	98.779	61.641	60.429
lab-crater-6	98.980	99.602	98.884	99.357	98.558	98.821	91.907	93.095
lab-crater-7	97.381	97.491	98.434	98.793	96.833	96.766	88.719	87.231

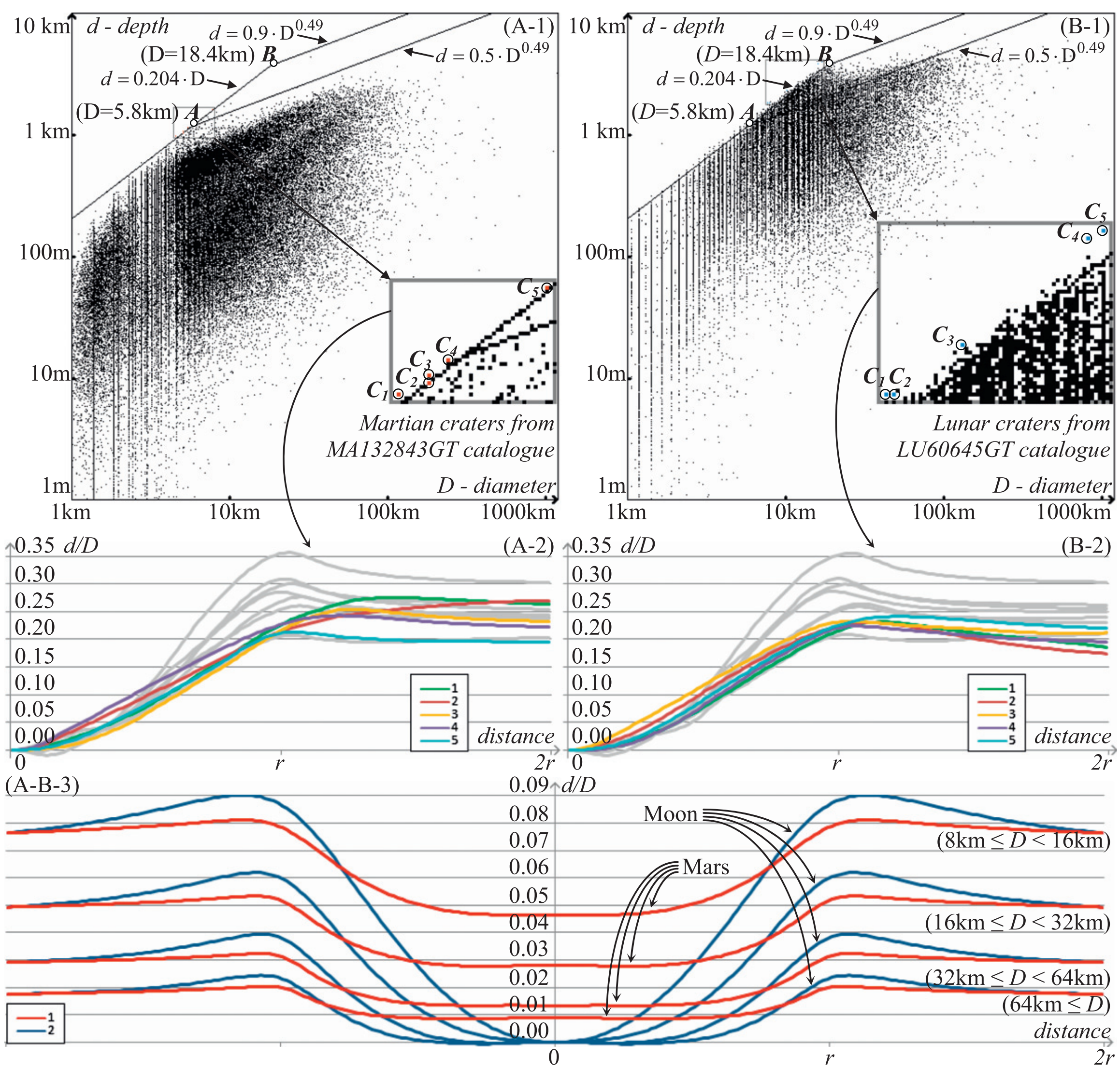

Fig. 9. Depth/diameter in log/log scale for Martian (A-1) and Lunar craters (B-1)—in each case five craters with some of the largest *d/D* ratios have been selected; comparison of profiles between laboratory and selected craters—these recent (with high *d/D* ratio) Martian (A-2) and Lunar (B-2) craters are similar to each other and to our laboratory craters; and the average profiles for four groups of craters (A-B-3) where, by contrast, there is a considerable difference between shallower Martian and deeper Lunar craters.

similar to craters, the hexagon is sufficiently similar, while the artificial objects triangle and quadrangle are somewhere between.

The measure of similarity between artificial and real craters, based on the A-ROC evaluation and Eq. (1), can be used in the second approximation for more detailed analysis. The results for Martian and Lunar test-fields and all four variations of CDA are shown in Table 3. The observations are as follows: (1) the A-ROC curve is not identical for cases when the test-field is (CDA computations need to be performed only once per selected CDA) or is not emplaced in target topography, however differences are small and can be ignored; (2) the measure of similarity between laboratory and real impact craters depends on the selected size of an emplaced laboratory crater, however this does not influence the results when all laboratory craters are scaled to the same size; (3) the 4th laboratory crater embedded in the Lunar test-filed is not detected via CDA_2-Shen-Castan when it is emplaced in the smallest size, therefore the conclusion is that for the Turing criteria it should be sufficient for passing the test that most detections are successful; (4) the overall measure of similarity is in some cases larger for mathematical models of craters than for laboratory or even real craters, we intentionally included this case in order to illustrate the potential overestimation

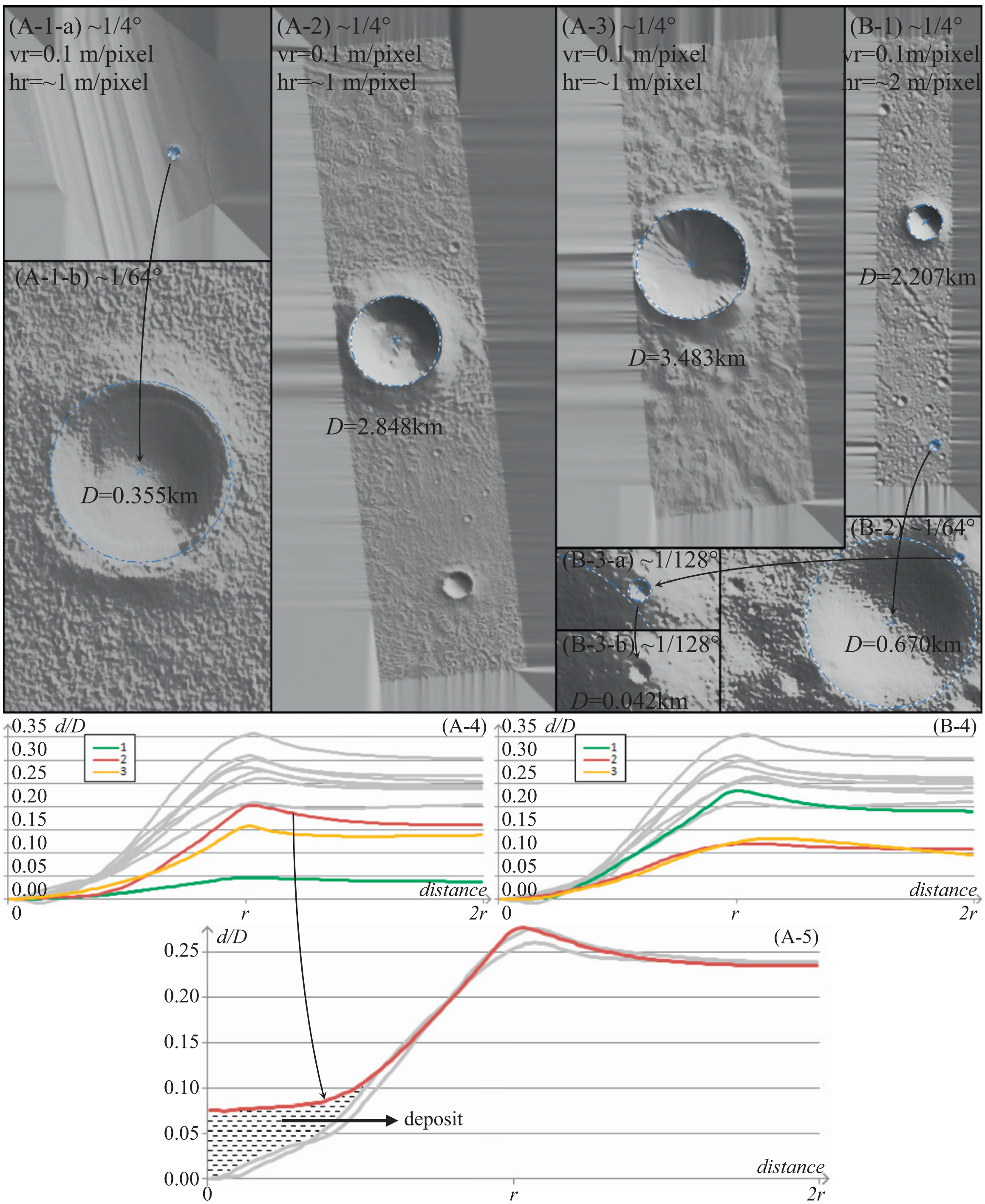

Fig. 10. Comparison of craters profiles from three Martian HiRISE (A-1, A-2, and A-3) and one Lunar LROC (B-1, B-2, and B-3) DEMs with profiles of laboratory craters (A-4, and B-4), and more detailed analysis in the case of Zumba crater—difference in profiles is most likely a deposit (A-5).

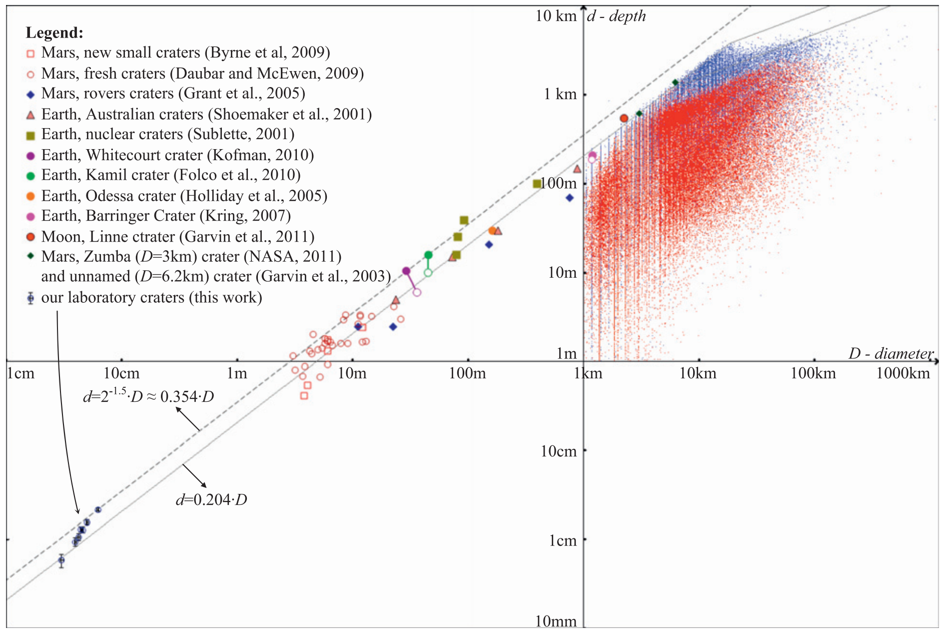

Fig. 11. Depth/diameter in log/log scale for all craters from LU60645GT catalog of Lunar craters (blue), MA132843GT catalog of Martian craters (red—superimposed over blue) and comparison with our laboratory craters and numerous other individual craters. (For interpretation of the references to color in this figure legend, the reader is referred to the web version of this article.)

problem; and (5) the resulting numbers are similar to each other and lead to similar conclusions whether we use Martian or Lunar test-field and which variation of CDA we use, this shows robustness and reliability of the overall approach.

3.7. Cross-comparison of profiles for standard and high horizontal resolutions

As noted in our previous work (Salamunićcar et al., 2012), there are some considerable differences between Martian and Lunar craters: (1) the transition of the depth/diameter ratio of the youngest craters on Mars occurs at $D=5.8$ km, while on the Moon it occurs at $D=18.4$ km, as shown in Fig. 9(A1 and B-1); (2) for Lunar craters the depth/diameter ratio and height of crater rim is approximately two times larger than for Martian craters, as shown in Fig. 9(A-B-3). However, the youngest (with highest depth/diameter ratio) Martian and Lunar craters do have, on the contrary, very similar profiles to each other and to the profiles of our laboratory craters, as shown in Figs. 9(A-2 and B-2). This confirms that our laboratory craters are good proxies for the scientific investigation of the youngest Martian and Lunar craters.

Using three Martian HiRISE and one Lunar LROC DEM, with much higher horizontal resolutions than available with global topography datasets, we additionally compared our laboratory craters with some craters that are much smaller than in the previous case, as shown in Fig. 10. One $D=2.848$ km large Martian crater (A-2) and one $D=2.207$ km large Lunar (B-1) crater have profiles with approximately the same depth/diameter ratio. In the case of the Zumba crater (A-2), the possibility of more detailed analysis is shown as well (A-5). When the profile is shifted in the graph upwards, it matches quite well the two profiles of laboratory craters for all distances between 0.5 and 2 radii. The difference is only for distances smaller than 0.5 radii. Our interpretation is that this difference is most likely a deposit, created after the formation of the transient crater. One possible application of the approach could be the impact melt volume estimates (Mazarico et al., 2011).

3.8. Depth/diameter ratio scaling

A depth/diameter in log/log scale for craters from recent Lunar and Martian catalogs and comparison with numerous other individual craters (Byrne et al., 2009; Daubar and McEwen, 2009; Folco et al., 2010; Garvin et al., 2003; Garvin et al., 2011; Grant et al., 2005; Holliday et al., 2005; Kofman, 2010; Kring 2007; NASA/JPL/University of Arizona, 2011; Shoemaker et al., 2001; Sublette, 2001) is shown in Fig. 11. Note how the largest depth/diameter ratio of the youngest craters is mostly independent of the crater's size and gravity despite many orders of magnitude of difference in crater depth or diameter. The transition between simple/small and complex/large craters is shown only at the top-right corner of Fig. 11. From this perspective as well, our laboratory craters are consistent with simple/small real impact craters on Mars, the Moon and Earth.

4. Conclusions

The result of this work is a complete framework for creation and evaluation of laboratory craters. The framework among others includes: (1) a new method for emplacement of laboratory craters in the topography of a planetary body; and (2) a new method for objective evaluation of laboratory craters which utilizes a CDA, the Turing test, and a new measure of similarity between laboratory and real craters. For the purpose of completeness, the framework also includes: (1) a procedure for creation of explosion-induced laboratory craters in stone powder surfaces using easily accessible silver acetylide (Ag_2C_2) for explosive charges; (2) a method for 3D scanning of laboratory craters using a GOM-ATOS-I 3D scanner; and (3) a possibility of accompanying manual evaluation of laboratory craters using 2D topographical profiles extracted using our previously developed CDA. The approach has been verified using Martian and Lunar test-fields, in combination with artificial objects and simplified mathematical models of craters. In addition, several craters from high-resolution Martian and Lunar DEMs have been compared with our laboratory craters, showing that scientific investigation of real impact craters using laboratory craters as proxies is possible for this case as well. Finally, the depth/diameter diagram in log/log scale of real impact craters on Mars, the Moon and Earth, with an extremely large range of depths and diameters, shows that our laboratory craters are consistent with real impact craters from this perspective as well. The major advantage of using the CDA for evaluation of laboratory craters, instead of, for example, a simple comparison of profiles, is that the CDA already has internal knowledge about craters' shapes, which can be utilized in order to achieve a higher quality of evaluation.

Acknowledgments

We thank Dominik Cinčić from the Department of Chemistry, Faculty of Science at the University of Zagreb for his help with preparation of explosive charges.

References

Ahrens, T.J., Xia, K., Coker, D., 2001. Depth of cracking beneath impact craters: new constraint for impact velocity. Shock Compression of Condensed Matter, 1393–1396.

Bandeira, L., Saraiva, J., Pina, P., 2007. Impact crater recognition on Mars based on a probability volume created by template matching. IEEE Transactions on Geoscience and Remote Sensing 45 (12), 4008–4015.

Bandeira, L., Ding, W., Stepinski, T.F., 2012. Detection of sub-kilometer craters in high resolution planetary images using shape and texture features. Advances in Space Research 49 (1), 64–74.

Bue, B.D., Stepinski, T.F., 2007. Machine detection of Martian impact craters from digital topography data. IEEE Transactions on Geoscience and Remote Sensing 45 (1), 265–274.

Barnouin-Jha, O.S., Cintala, M.J., Crawford, D.A., Anderson, J.L.B., Yamamoto, S., Sugita, S., 2007. Effects of target properties on the formation of laboratory scale impact craters. In: Proceedings of the Bridging the Gap II: Effect of Target Properties on the Impact Cratering Process. p. 8059. Abstract.

Burchell, M.J., Grey, I.D.S., Shrine, N.R.G., 2001. Laboratory investigations of hypervelocity impact cratering in ice. Advances in Space Research 28 (10), 1521–1526.

Burchell, M.J., Leliwa-Kopystyński, J., Arakawa, M., 2005. Cratering of Icy Targets by Different Impactors: Laboratory Experiments and Implications for Cratering in the Solar System. Icarus, 179. Elsevier. (1), 274-288.

Burl, M.C., Wetzler, P.G., 2011. Onboard object recognition for planetary exploration. Machine Learning 84 (3), 341–367.

Byrne, S., Dundas, C.M., Kennedy, M.R., Mellon, M.T., McEwen, A.S., Cull, S.C., Daubar, I.J., Shean, D.E., Seelos, K.D., Murchie, S.L., Cantor, B.A., Arvidson, R.E., Edgett, K.S., Reufer, A., Thomas, N., Harrison, T.N., Posiolova, L.V., Seelos, F.P., 2009. Distribution of mid-latitude ground ice on Mars from new impact craters. Science 325 (5948), 1674–1676.

Cintala, M.J., Berthoud, L., Hörz, F., 1998. Impact craters in the laboratory: relationships between impact and ejection velocities. In: Proceedings of the 29th Lunar and Planetary Science Conference, p. 1813. Abstract [CDROM].

Claycomb, J.R., 2009. Impact crater experiments for introductory physics and astronomy laboratories. Physics Education 44 (2), 184–187.

Collins, G.S., Melosh, H.J., Marcus, R.A., 2005. Earth impact effects program: a web-based computer program for calculating the regional environmental consequences of a meteoroid impact on earth. Meteoritics & Planetary Science 40 (6), 817–840.

Cooper, G.R.J., Cowan, D.R., 2004. The detection of circular features in irregularly spaced data. Computers & Geosciences 30 (1), 101–105.

Cross, A.M., 1988. Detection of circular geological features using the Hough transform. International Journal of Remote Sensing 9 (9), 1519–1528.

Daubar, I.J., McEwen, A.S., 2009. Depth to diameter ratios of recent primary impact craters on Mars. In: Proceedings of the 40th Lunar and Planetary Science Conference, p. 2419. Abstract [CDROM].

Davison, T.M., Collins, G.S., Elbeshausen, D., Wünnemann, K., Kearsley, A., 2011. Numerical modeling of oblique hypervelocity impacts on strong ductile targets. Meteoritics & Planetary Science 46 (10), 1510–1524.

Desai, T., Batani, D., Bussoli, M., Villa, A.M., Dezulian, R., Krousky, E., 2007. Laboratory craters to meteorite complex-craters, can we? In: Proceedings of the 3rd International Conference on the Frontiers of Plasma Physics and Technology. Abstract.

Desai, T., Batani, D., Bussoli, M., Villa, A.M., Dezulian, R., Krousky, E., 2008. Laboratory craters: modeling experiments for meteorite impact craters? IEEE Transactions on Plasma Science 36 (4), 1132–1133.

Desai, T., Bussoli, M., Dezulian, R., Villa, A., Krousky, E., Aliverdiev, A.A., Kubkowska, M., Wolowski, J., 2010. Analogy of meteorite impacts in laboratory conditions. Physica Scripta 2010 (T142), 5.

Ding, W., Stepinski, T.F., Mu, Y., Bandeira, L., Ricardo, R., Wu, Y., Lu, Z., Cao, T., Wu, X., 2011. Sub-kilometer crater discovery with boosting and transfer learning. ACM Transactions on Intelligent Systems and Technology 2 (4), 1–22.

Fechtig, H., Gault, D.E., Neukum, G., Schneider, E., 1972. Laboratory simulation of lunar craters. Naturwissenschaften 59 (4), 151–157.

Flores-Méndez, A., Suarez-Cervantes, A., 2009. Circular degree Hough transform. Lecture Notes in Computer Science 5856, 287–294.

Folco, L., Di Martino, M., El Barkooky, A., D'Orazio, M., Lethy, A., Urbini, S., Nicolosi, I., Hafez, M., Cordier, C., van Ginneken, M., Zeoli, A., Radwan, A.M., El Khrepy, S., El Gabry, M., Gomaa, M., Barakat, A.A., Serra, R., El Sharkawi, M., 2010. The Kamil Crater in Egypt (Brevia). Science 329 (5993), 804.

French, B.M., 1998. Traces of Catastrophe. 〈http://www.lpi.usra.edu/publications/books/CB-954/CB-954.intro.html〉, (accessed: 23.12..11).

Garvin, J.B., Sakimoto, S.E.H., Frawley, J.J., 2003. Craters on Mars: global geometric properties from gridded MOLA topography. In: Proceedings of the Sixth International Conference on Mars, p. 3277. Abstract [CDROM].

Garvin, B., Robinson, M.S., Frawley, J., Tran, T., Mazarico, E., Neumann, G., 2011. Linne: simple lunar mare crater geometry from LRO observations. In: Proceedings of the 42nd Lunar and Planetary Science Conference, p. 2063. Abstract [CDROM].

GOM, 2012. ATOS Compact Scan, the Compact Class of Scanning. 〈http://www.gom.com/metrology-systems/system-overview/atos-compact-scan.html〉, (accessed: 19.01.12)..

Grant, J.A., Golombek, M.P., Haldemann, A.F.C., Crumpler, L., Li, R., Watters, W.A., 2005. Field studies of crater gradation in Gusev crater and meridiani planum using the Mars Exploration Rovers. In: Proceedings of the Workshop on the Role of Volatiles and Atmospheres on Martian Impact Craters, p. 3004. Abstract [CDROM].

Grey, I.D.S., Burchell, M.J., Shrine, N.R.G., 2001. Laboratory investigations of the temperature dependence of hypervelocity impact cratering in ice. Advances in Space Research 28 (10), 1527–1532.

Grieve, R.A.F., 1987. Terrestial impact structures. Annual Review of Earth and Planetary Sciences 15, 245–270.

Holliday, V.T., Kring, D.A., Mayer, J.H., Goble, R.J., 2005. Age and effects of the Odessa meteorite impact, western Texas, USA. Geology 33 (12), 945–948.

Herrick, R.R., Yamamoto, S., Barnouin-Jha, O.S., Sugita, S., Matsui, T., 2008. Constraints from laboratory experiments on crater excavation and formation of an uprange forbidden zone in an oblique impact. In: Proceedings of the 39th Lunar and Planetary Science Conference, p. 2305. Abstract [CDROM].

Hiraoka, K., Arakawa, M., Yoshikawa, K., Nakamura, A.M., 2007. Laboratory experiments of crater formation on ice silicate mixture targets. Advances in Space Research 39 (3), 392–399.

Holsapple, K.A., 1993. The scaling of impact processes in planetary sciences. Annual Review of Earth and Planetary Sciences 21, 333–373.

Holsapple, K.A., 1994. Recipes for impact cratering. In: Proceedings of the 25th Lunar and Planetary Science Conference, p. 559. Abstract [CDROM].

Kasas, S., Dumas, G., Dietler, G., 2000. Impact cratering study performed in the laboratory without a fast recording camera. American Journal of Physics 68 (8), 771–773.

Kim, J.R., Muller, J.-P., van Gasselt, S., Morley, J.G., Neukum, G., 2005. Automated crater detection, a new tool for Mars cartography and chronology. Photogrammetric Engineering & Remote Sensing 71 (10), 1205–1217.

Kofman, R.S., 2010. An Investigation of the Whitecourt Meteorite Impact Crater (Alberta, Canada). Master of Science Thesis, University of Alberta, Canada, pp. 1–83.

Kring, D.A., 2007. Guidebook to the Geology of Barringer Meteorite Crater, Arizona (a.k.a. Meteor Crater). 〈http://www.lpi.usra.edu/publications/ books/barringer_crater_guidebook/crater_guidebook.pdf〉, (accessed date: 23.12.11).

Krøgli, S.O., Dypvik, H., 2010. Automatic detection of circular outlines in regional gravity and aeromagnetic data in the search for impact structure candidates. Computers & Geosciences 36 (4), 477–488.

Leroy, B., Medioni, G., Johnson, E., Matthies, L., 2001. Crater detection for autonomous landing on asteroids. Image and Vision Computing 19 (11), 787–792.

Liu, S., Ding, W., Stepinski, T.F., 2011. Semi-supervised active class selection for automatic identification of sub-kilometer craters. In: Proceedings of the 7th International Symposium on Image and Signal Processing and Analysis, pp. 615–620.

Maass, B., Krüger, H., Theil, S., 2011. An edge-free, scale-, pose- and illumination-invariant approach to crater detection for spacecraft navigation. In: Proceedings of the 7th International Symposium on Image and Signal Processing and Analysis, pp. 603–608.

Martins, R., Pina, P., Marques, J.S., Silveira, M., 2009. Crater detection by a boosting approach. IEEE Geoscience and Remote Sensing Letters 6 (1), 127–131.

Mazarico, E., Barnouin, O.S., Salamunićcar, G., Zuber, M.T., 2011. Impact melt volume estimates of small- to medium-sized Lunar craters from Lunar Reconnaissance Orbiter data. In: Proceedings of the 42nd Lunar Planetary Science Conference, p. 2075. Abstract [CDROM].

Melosh, H.J., Ivanov, B.A., 1999. Impact crater collapse. Annual Review of Earth and Planetary Sciences 27, 385–415.

Michael, G.G., 2003. Coordinate registration by automated crater recognition. Planetary and Space Science 51 (9–10), 563–568.

Milner, D.J., Baldwin, E.C., Burchell, M.J., 2008. Laboratory investigations of marine impact events: factors influencing crater formation and projectile survivability. Meteoritics & Planetary Science 43 (12), 2015–2026.

Miljković, K., Mason, N.J., Zarnecki, J.C., 2011. Ejecta fragmentation in impacts into gypsum and water ice. Icarus 214 (2), 739–747.

NASA/JPL/University of Arizona, 2011. Zumba Crater: Fresh 3 km Crater with Impressive Ejecta and Ray Pattern. 〈http://hirise.lpl.arizona.edu/PSP_003608_1510〉, (accessed: 24.11.2011).

Ormö, J., 2005. The influence of water on the cratering and modification of marine-target craters—some thoughts based on recent field studies and laboratory experiments. In: Proceedings of the Role of Volatiles and Atmospheres on Martian Impact Craters, p. 3023. Abstract.

Polanskey, C.A., Ahrens, T.J., 1990. Impact spallation experiments: fracture patterns and spall velocities. Icarus 87 (1), 140–155.

Ransom, C.J., 2011. Laboratory modeling of meteorite impact craters by Z-pinch plasma. The Open Astronomy Journal 4 (1), 185–190.

Schmidt, R.M., Holsapple, K.A., 1980. Theory and experiments on centrifuge cratering. Journal of Geophysical Research—Solid Earth 85 (B1), 235–252.

Salamunićcar, G., Lončarić, S., 2010. Method for crater detection from Martian digital topography data using gradient value/orientation, morphometry, votes-analysis, slip-tuning and calibration. IEEE Transactions on Geoscience and Remote Sensing 48 (5), 2317–2329.

Salamunićcar, G., Vinković, D., Lončarić, S., Vučina, D., Pehnec, I., Vojković, M., Gomerčić, M., Hercigonja, T., 2010. Method for evaluation of laboratory craters using crater detection algorithm for digital topography data. In: Proceedings of 38th the COSPAR Scientific Assembly, p. B02-0044-10. Abstract [CDROM].

Salamunićcar, G., Lončarić, S., 2011. Framework for Evaluation of Crater Detection Algorithms—FECDA2011B. 〈http://www.fer.unizg.hr/ipg/research/fecda〉 and 〈http://fecda.crocserve.com/〉.

Salamunićcar, G., Lončarić, S., Mazarico, E., 2012. LU60645GT and MA132843GT catalogues of Lunar and Martian impact craters developed using a Crater Shape-based interpolation crater detection algorithm for topography data. Planetary and Space Science 60 (1), 236–247.

Sawabe, Y., Matsunaga, T., Rokugawa, S., 2006. Automated detection and classification of lunar craters using multiple approaches. Advances in Space Research 37 (1), 21–27.

Saygin, A.P., Cicekli, I., Akman, V., 2000. Turing test: 50 years later. Minds and Machines 10 (4), 463–518.

Senft, L.E., Stewart, S.T., 2007. Modeling impact cratering in layered surfaces. Journal of Geophysical Research—Planets 112 (E11), 18.

Shoemaker, E.M., Macdonald, F.A., Shoemaker, C.S., 2001. Geology of five small Australian impact craters. Australian Journal of Earth Sciences 52 (4–5), 529–544.

Smith, D., Neumann, G., Arvidson, R.E., Guinness, E.A., Slavney, S., 2003. Mars Global Surveyor Laser Altimeter Mission Experiment Gridded Data Record. NASA Planetary Data System.

Smith, D.E., Zuber, M.T., Neumann, G.A., Lemoine, F.G., Mazarico, E., Torrence, M.H., McGarry, J.F., Rowlands, D.D., Head III, J.W., Duxbury, T.H., Aharonson, O., Lucey, P.G., Robinson, M.S., Barnouin, O.S., Cavanaugh, J.F., Sun, X., Liiva, P., Mao, D.d., Smith, J.C., Bartels, A.E., 2010. Initial observations from the Lunar Orbiter Laser Altimeter (LOLA). Geophysical Research Letters 37, 1–6. (L18204).

Stepinski, T.F., Urbach, E.R., 2008. Completion of the first automatic survey of craters on Mars. In: Proceedings of the 11th Mars Crater Consortium meeting, US Geological Survey in Flagstaff-AZ.

Stepinski, T.F., Mendenhall, M.P., Bue, B.D., 2009. Machine cataloging of impact craters on Mars. Icarus 203 (1), 77–87.

Sublette, C., 2001. The Effects of Underground Explosions. 〈http://nuclearweaponarchive.org/Library/Effects/UndergroundEffects.html〉, (accessed: 24.11.11).

Suzuki, A., Kumagai, I., Nagata, Y., Kurita, K., Barnouin-Jha, O.S., 2007. Modes of ejecta emplacement at Martian craters from laboratory experiments of an expanding vortex ring interacting with a particle layer. Geophysical Research Letters 34 (5), 5.

Taud, H., Parrot, J.F., 1992. Detection of circular structures on satellite images. International Journal of Remote Sensing 13 (2), 319–335.

Troglio, G., Le Moigne, J., Benediktsson, J.A., Moser, G., Serpico, S.B., 2012. Automatic extraction of ellipsoidal features for planetary image registration. IEEE Geoscience and Remote Sensing Letters 9 (1), 95–99.

Urbach, E.R., Stepinski, T.F., 2009. Automatic detection of sub-km craters in high resolution planetary images. Planetary and Space Science 57 (7), 880–887.

Vinković, D., Salamunićcar, G., Lončarić, S., Vučina, D., Gomerčić, M., Pehnec, I., Vojković, M., Hercigonja, T., 2011. Test-field for evaluation of laboratory craters using interpolation-based crater detection algorithm and comparison with Martian impact craters. In: Proceedings of the 42nd Lunar and Planetary Science Conference, p. 1453. Abstract [CDROM].

Vojković, M., Karbonini, L., Vinković, D., Salamunićcar, G., Lončarić, S., 2010a. Laboratory craters and their comparison with craters from GT-115225 global catalogue of Martian impact craters. In: Proceedings of the 41st Lunar and Planetary Science Conference, p. 1428. Abstract [CDROM].

Vojković, M., Pehnec, I., Vučina, D., Vinković, D., Salamunićcar, G., Lončarić, S., Gomerčić, M., Hercigonja, T., 2010b. 3D topography of laboratory craters and their comparison with Martian impact craters. In: Proceedings of the 38th COSPAR Scientific Assembly, p. B02-0052-10. Abstract [CDROM].

Wan, C., Cheng, W.M., Zhou, Z.P., Zhao, S.M., Xia, Y., 2012. Automatic extraction of lunar impact craters from Chang'E-1 satellite photographs. Science China: Physics, Mechanics and Astronomy 55 (1), 162–169.

Wang, Y., Ding, W., Yu, K., Wang, H., Wu, X., 2011. Crater detection using Bayesian classifiers and LASSO. In: Proceedings of the IEEE International Conference on Intelligent Computing and Integrated Systems, pp. 1–5.